

## CRATER BOUGUER ANOMALIES PROBE SOUTH-POLE-AITKEN (SPA) BASIN STRUCTURE.

Roger J. Phillips<sup>1</sup>, Carver J. Thomason<sup>2</sup>, James W. Head III<sup>3</sup>, Jason M. Soderblom<sup>4</sup>, Francis Nimmo<sup>2</sup>, Jonathan Bes-serer<sup>5</sup>, H. Jay Melosh<sup>6</sup>, Colleen Milbury<sup>6</sup>, Walter S. Kiefer<sup>7</sup>, and Maria T. Zuber<sup>4</sup>. <sup>1</sup>Planetary Science Directorate, Southwest Research Institute, Boulder, CO 80302, USA (roger@boulder.swri.edu); <sup>2</sup>Dept. of Earth and Planetary Sciences, University of California, Santa Cruz, CA 95064, USA; <sup>3</sup>Dept. of Earth, Environmental and Planetary Sciences, Brown University, Providence, RI 02912, USA; <sup>4</sup>Dept. of Earth, Atmospheric and Planetary Sciences, Massachusetts Institute of Technology, Cambridge MA 02139, USA; <sup>5</sup>Laboratoire de Planétologie et Géodynamique de Nantes, Université de Nantes, France; <sup>6</sup>Department of Earth, Atmospheric, and Planetary Sciences, Purdue University, West Lafayette, IN 47907, USA; <sup>7</sup>Lunar and Planetary Institute, Houston, TX 77058, USA.

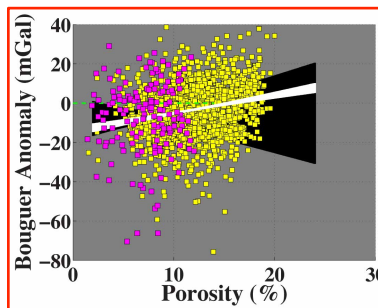
**Introduction.** One of the primary objectives of the Gravity Recovery and Interior Laboratory (GRAIL) mission [1] was to use the Bouguer gravity signals of impact craters to not only learn about the subsurface disposition beneath craters (e.g., extent of brecciation), but also to use these crater gravity signals as probes into the structure of the crust and upper mantle. Such investigations will help us to better understand the interplay of competing processes (e.g., impacts, magmatism) during the evolution of the outer part of the Moon.

Here we examine the spatial distribution of complex crater Bouguer anomalies ( $BA$ ), with a particular emphasis on contrasting gravity anomalies in the South Pole-Aitken (SPA) basin with their counterparts in the lunar highlands. We also examine the statistical behavior of crater  $BA$  as a function of crater diameter ( $D$ ) and background regional porosity ( $\phi$ ), contrasting behavior within and outside SPA.

**Context.** We examine complex craters over the diameter range 30 to 150 km – the low end a practical resolution limit and the high-end selected to avoid effects of mantle uplift.  $BA$  signals associated with complex craters are generally messy largely due to contributions from other geological structures. Examining ensembles of craters, either spatially or statistically, reveals trends that provide insight into the origin of the  $BA$  signal, particularly when filters are applied to remove the geologically noisiest craters from the data [2]. Although  $BA$  signals are scattered when plotted against diameter, trends emerge that are statistically meaningful. This includes a negative linear slope in  $BA-D$  plot (Figure 2), indicating that as a global ensemble, the  $BA$  reflects a  $D$ -dependent mass deficiency, and a break in slope (beyond the data range in Figure 2) that may be indicative of the depth of fracture closing in the crust [3]. Still, there is abundant scatter in this relationship and for almost any diameter there are both positive and negative anomalies. Using hydrocode simulations, Milbury [4] showed that such scatter is directly related to the background porosity that hosts the impact. Additionally, bulk density and porosity as a function of depth have been derived from

localized spectral admittances [5], and these results influence the work presented here. Finally, spectral studies have recently focused on SPA to test specific models of vertical density structure [6], including the necessity of a large melt sheet [7].

**Results.** Figure 1 plots  $BA$  against porosity inside and outside SPA. There is a statistically significant (see Table 1) positive trend outside of SPA [3], as predicted by [4], and no such trend in the SPA data, which



is limited to low porosities.

**Figure 1.** Scatter plot of  $BA$  vs. porosity inside (magenta) and outside (yellow) SPA, with, respectively, black and white 95% confidence

bands on a linear fit. Porosity,  $\phi$ , was determined from a grain density,  $\rho_g$ , model [8] and a bulk density model [5],  $\rho_b(z) = \rho_{\text{surf}} + \Delta\rho(1 - e^{-z/d})$ , where  $d$  is the e-folding depth and  $\Delta\rho$  is the fractured-unfractured density contrast. Mean values of  $\phi$ , for  $z = 5$  km, were estimated in an annulus between  $D$  and  $1.5D$  surrounding each crater. Thus the background (regional) porosity is a crater property.

$BA$ vs. $\phi$	Depth, $z$ (km)		
	5	7.5	10
<i>Outside SPA slope</i>	0.92	0.79	0.73
<i>Outside SPA p-val.</i>	2.2E-28	6.9E-28	1.2E-25
<i>Inside SPA slope</i>	0.12	-0.25	-0.63
<i>Inside SPA p-val.</i>	3.9E-01	3.8E-01	3.2E-01

**Table 1.** Statistical results of linear fits of  $BA$  vs.  $\phi$ . Slope units are mGal/porosity. The  $p$ -value tests the null hypothesis that the slope is zero.

The  $BA-D$  relationship (Figure 2) shows that the magnitude of the negative slope in SPA is 2.5 times that of the rest of the Moon (Table 2). This is easy to understand given the low values of  $\phi$  in SPA. If the  $BA-D$  relationship can be expressed as a power law, then the Bouguer anomaly is given by  $g_B = C\Delta\rho D^n$ , where  $C$  and  $n$  are constants and  $\Delta\rho$  is the density con-

trast between the crater's subsurface and the surrounding terrain. If  $\Delta\phi$  is the corresponding porosity contrast, the  $BA$ - $D$  slope is  $dg_B/dD = nC\rho_g\Delta\phi D^{n-1}$ , where  $\rho_g$  is the grain density. Given the dominance of low porosities (Figure 1),  $\Delta\phi$  values in SPA are large relative to the rest of the Moon and the increased slope is expected (Figure 2).

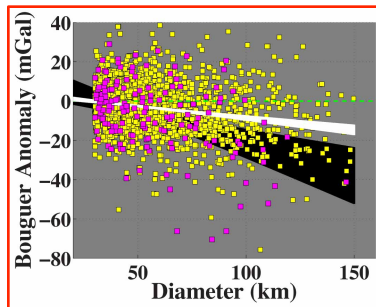


**Figure 2.** Scatter plot of  $BA$  vs.  $D$  inside (magenta) and outside (yellow) the SPA, with, respectively, black and white 95% confidence bands.

Slope: $BA$ vs. $D$		$p$ -values	
Outside SPA	-0.13	Outside SPA	1.3E-33
Inside SPA	-0.32	Inside SPA	3.7E-09
Use regional value in Bouguer correction:			
Outside SPA	-0.11	Outside SPA	1.6E-23
Inside SPA	-0.27	Inside SPA	1.2E-05

**Table 2.** Statistical results of linear fits of  $BA$  vs.  $D$ . Bouguer anomalies in the work presented here were calculated using a single global density ( $2.56 \text{ Mg/km}^3$ ) for the Bouguer corrections. The bottom two rows show that using the regional value surrounding a crater for the correction leads to a small change in the results. Slopes are  $\text{mGal/km}$ .

Figure 3 shows the spatial distribution of impact craters in our 4000+ crater database that fall within the diameter range 30–150 km, that survived a geological noise filter, and that have  $BA$  magnitudes  $> 10 \text{ mGal}$ . The are plotted over a map of porosity ( $z = 5 \text{ km}$  [5]) and color-coded for anomaly sign (+ = magenta, - = green). There is a clear association of  $-BA$  with regions of low porosity as expected from Figure 1 and as predicted from hydrocode simulations [4]. There is nothing particularly unique about SPA, meaning that there are spatially coherent regions in the highlands that are dominated by  $-BA$  and are associated with low porosity.

As Besserer et al. [5] emphasized, what sets SPA apart from the highlands is a thinner (smaller e-folding depth,  $d$ ) low density layer. This can be seen in Figure 4, which shows the crater distribution over a map of bulk density at 5-km depth. Clearly at this depth, the SPA rocks are closer to their unfractured state than those of the highlands. As adopted to point crater properties, the linear bulk density vertical gradient [5] in SPA is on average 50% higher than elsewhere.

**Path Forward.** Our working hypothesis is that the post-SPA formation impact energy flux had declined to the point of inducing “little” dilatancy into the extant rock mass, thus explaining the low porosity and  $BA$  vs.  $D$  in SPA. Furthermore, we propose that the SPA formation event itself was effective at removing existing dilatancy (e.g., formation of a thick melt sheet). Our path forward is to model the Bouguer signals for individual craters employing vertical density variations beneath both the crater and in the surrounding terrain. Additionally, we will convolve dilatancy models [9] with bombardment models [e.g., 10] in an attempt to constrain the relative timing of SPA formation and the lunar bombardment history.

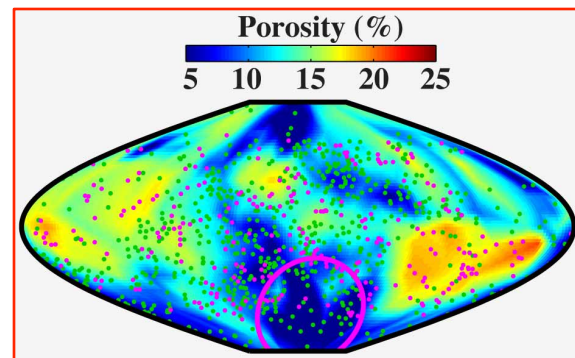


**Figure 3.**  $BA$  crater locations coded for anomaly sign (+ = magenta, - = green) superposed on a porosity map [5] at 5-km depth. Magenta circle indicates SPA basin. Sinusoidal projection;  $180^\circ\text{E}$  at center of map.

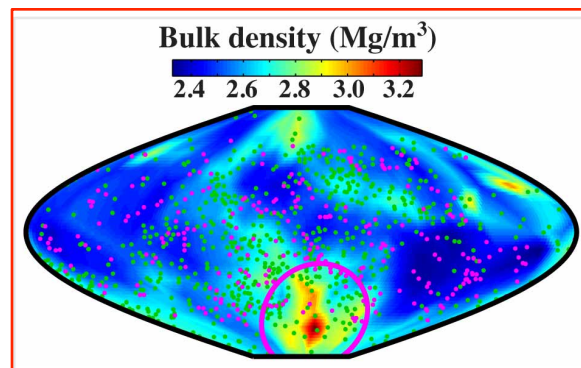


**Figure 4.**  $BA$  crater locations coded for anomaly sign (+ = magenta, - = green) superposed on a bulk density map [5] at 5-km depth. Sinusoidal projection;  $180^\circ\text{E}$  at center of map.

**References:** [1] Zuber M. T. et al. (2013) *Science* 339, 668–671. [2] Thomason C. J. et al. (2015) *JGR Planets*, in prep. [3] Soderblom J. M. (2015) *Nature*, submitted. [4] Milbury C. et al. (2015) LPSC 46, Abs. #1966. [5] Besserer J. et al. (2014) *Geophys. Res. Lett.* 41, 5771–5777. [6] Ertel A. (2014) *AGU Fall Meeting*, paper G22A-04. [7] Vaughan W. M. and Head J. W. III (2014) *Planet. Space Sci.*, 91, 101–106. [8] Wieczorek M. A. et al. (2013) *Science* 339, 671–675. [9] Collins G. S. (2014) *JGR Planets* 119, doi:10.1002/2014JE004708. [10] Morbidelli A. et al. (2012) *EPSL* 355-356 (2012) 144–151.